Deep–Sea Research II 218 (2024) 105431

Contents lists available at ScienceDirect

Deep-Sea Research Part II

journal homepage: www.elsevier.com/locate/dsr2

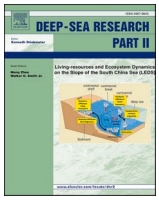

Methane distribution above the Emperor Seamount chain

Nikita S. Polonik *, Alexey A. Legkodimov

V.I. Il'ichev Pacific Oceanological Institute (POI), FEB RAS, Baltiyskaya 43, 690041, Vladivostok, Russian Federation

A R T I C L E I N F O

Handling Editor: Dr W Smith

Keywords:
Northwestern Pacific
Dissolved methane
Seamounts
Emperor chain
Water column
Guyots

A B S T R A C T

Dissolved methane (CH_4) concentrations were measured in the water column at 25 stations along the four sections above Koko and Jingu guyots (the southern part of Emperor Seamount chain). The measured methane concentrations were relatively low (1–6.5 nM). The patterns of CH_4 vertical distributions over Koko and Jingu were different. The greatest dissolved methane concentrations (6.5 nM) were found in the near-bottom layer (357 m) above the Koko summit. For Koko guyot, the greatest CH_4 content (3.9–6.5 nM) was mainly associated with the subsurface (10–300 m) layer above the summit. However, another methane plume (6 nM) was detected at 1000 m on the western slope of the guyot. We propose that methane maximum was caused by the influence of the Kuroshio Extension or deep eddies. The CH_4 distribution over Jingu gyuot was similar to that in open ocean waters. The greatest methane concentrations (3.8–6 nM) were found in the subsurface layers above the summit. Methane exceeded atmospheric equilibrium concentration in the surface (5–52 % supersaturation) layer for both Koko and Jingu. The methane content and supersaturation level in the subsurface layer was at least two times higher than previously measured values for the open ocean. We believe that the high methane and supersaturation level was caused by enhanced methanogenesis in the water column above the seamounts. The estimated methane flux to the atmosphere varied from 1.4 to 16.3 μmol m^{-2} day^{-1} for Koko and from 0.5 to 6.5 μmol m^{-2} day^{-1} for Jingu, respectively. The average fluxes calculated for Koko (8.37 μmol m^{-2} day^{-1}) and Jingu (2.8 μmol m^{-2} day^{-1}) were significantly greater than the average flux for open and coastal oceans. Given the substantial methane atmospheric contributions, the global methane budget should be reconsidered.

1. Introduction

Methane is a powerful greenhouse gas (Van Amstel, 2012; Mar et al., 2022), playing an important role in the global carbon cycle. The steady increase of CH_4 concentrations in the atmosphere from 1610 to 1904 ppb has been observed over the past few decades (Lan et al., 2023), although the causes and mechanisms of this phenomenon are not completely understood (Canadell et al., 2021). For the World Ocean a total emission of methane into the atmosphere varies from 6 to 12 Tg yr^{-1}(Weber et al., 2019). The natural sources of CH_4 in oceans have geological (mud volcanoes, hydrothermal vents and cold seeps, faults, oil and gas deposits; Etiope and Schwietzke, 2019), hydrate (gas hydrate and permafrost dissociation; Archer et al., 2009), biological (methanogenesis in sea water; Bogard et al., 2014) and sedimentary (Ferry and Lessner, 2008) origins. The ocean may also be considered as the largest natural methane reservoir where the complex processes of biosynthesis (Reeburgh, 2007), emission (Hamdan and Wickland, 2016) and utilization (Mao et al., 2022) take place. The surface layers of the Pacific, Atlantic, Indian and Arctic oceans are considered as weak sources of methane to the atmosphere. Only the Southern Ocean, as well as a northern part of Atlantic Ocean, are weak sink for methane (Weber et al., 2019).

The main focus of studies of methane sources and sinks in the Northwestern Pacific are mainly directed to the Sea of Japan (Vereshchagina et al., 2013), Sea of Okhotsk (Yoshida et al., 2004; Sokolova et al., 2021), Bering Sea (Kosmach et al., 2015) and East China Sea (Sun et al., 2015; Toki et al., 2023). The marginal seas of the Northwestern Pacific have unique geological settings including a long chain of active volcanoes, tectonic belts (Kuril-Kamchatka arc, Setouchi volcanic belt), faults and fault zones. Moreover, there are numerous oil and gas deposits in the Sea of Okhotsk and East China Sea (Wang et al., 2019). Finally, some of these seas are considered as a promising source for the exploration of the methane gas hydrates (Matveeva et al., 2022; Jin et al., 2011; Hiruta and Matsumoto, 2022).

Despite the progress in our understanding of the features of CH_4 emission, distribution and biosynthesis in the marginal seas, the non-

* Corresponding author.
E-mail address: nikpol@poi.dvo.ru (N.S. Polonik).

https://doi.org/10.1016/j.dsr2.2024.105431
Received 26 March 2024; Received in revised form 30 September 2024; Accepted 16 October 2024
Available online 16 October 2024

coastal Pacific Ocean is less studied. Few works have been focused on methane distributions in surface and deep waters (Tilbrook and Karl, 1995; Watanabe et al., 1995; Kelley and Jeffrey, 2002; Pack et al., 2015; Chronopoulou et al., 2017). These studies revealed the presence of the dissolved methane maximum in upper oxic waters and oversaturation of the surface mixed layer. The phenomenon is called "the methane paradox" and may be caused by numerous factors (Bižić et al., 2020a). For open waters, the "methane paradox" is a result of methylphosphonate microbial utilization (Ye et al., 2020), and *in situ* CH_4 biosynthesis by cyanobacteria (Bižić et al., 2020b), phytoplankton (Weller et al., 2013) and algae (Klintzsch et al., 2019). However, further studies of the "methane paradox" phenomenon in open oceanic areas are necessary for the better understanding of the origin of natural CH_4 sources and the global methane budget.

In the northwestern Pacific the Emperor volcanic seamounts are of special interest (Clark et al., 2011) for fisheries, geological (Chen et al., 2021) and ecological investigations (Dautova et al., 2019). The Emperor chain (EC) extends from ~20°N to 50°N with a length of more 6000 km. The chain consists of numerous guyots (eroded flat-topped seamounts of volcanic origin). The summit depth of the seamounts varied from 18 (Kinmei guyot) to 1550 m (Detroit guyot; Roden et al., 1982). The main features of seamount hydrology are connected with circulation (Komaki and Kawabe, 2009), eddies (Vastano et al., 1985; Bograd et al., 1997) and Taylor column formation (Roden and Taft, 1985). A Taylor column is a fluid dynamics phenomenon caused by the Coriolis effect. It is a hydrological structure around seamount usually represented by anticyclonic eddy, uplifting of the isopycnals and the formation of a relatively stationary water column trapped over the top of the seamount (White and Mohn, 2004). Taylor columns generate a local upwelling and the transfer of nutrients from depth to the surface layers and entrapment of the nutrients over the seamount summit (Kiriakoulakis and Wolff, 2005). Due to the great impact of Taylor columns on seamount ecosystems, primary production, thermohaline parameters, macro- and micronutrients distribution and seawater circulation (Rogers, 2018), many studies have focused on confirming the existence of this hydrological phenomenon above seamounts (White and Mohn, 2004; Marsac et al., 2020; Ma et al., 2021). The influence of seamounts is often referred to as "the seamount effect" but also could be associated with other types of flow-topography interactions such as seamount-induced upwelling, formation of mesoscale eddies and deflection of major oceanic currents.

The main biogeochemical features of the "seamount effect" are connected with the redistribution of macro- and micronutrients in the water column and acceleration of sedimentation processes (Turnewitsch et al., 2013). Thus, the "seamount effect" is regarded as an enhanced (Yang et al., 2020) or weak (Ota et al., 2022) bioturbation on the summit, retention and accumulation of particulate organic carbon (POC) on the flanks of seamount (Vilas et al., 2009), POC production (Djurhuus et al., 2017), export and localization (Turnewitsch et al., 2016). These processes lead to the growth and development of microbes (Mendonça et al., 2012; Busch et al., 2020) and planktonic communities (Dai et al., 2020, 2022; Zhao et al., 2022, 2023) around the summit and an increase in the diversity of the ecosystem (Boehlert, 1988). Today, seamounts are often considered a "hotspot" of life in the oligotrophic ocean, and it could be expected that the seamounts are also a "hotspot" for CH_4 synthesis and emission. However, little is known about the influence of seamounts on CH_4 distribution, production and sinks.

The EC is an interesting area for the study of spatial methane distribution in the water column because of its remoteness to the common CH_4 sources typical for marginal seas such as marine sediments, cold methane seeps, oil, gas and gas hydrate deposits. EC is regarded as a barrier to the Kuroshio Extension (Roden et al., 1982) and subarctic gyre of the North Pacific (Wagawa et al., 2012; Kono and Kawasaki, 1997). However, the existence of a Taylor column was clearly identified only for Nintoku (Wagawa et al., 2012) guyot, and anticyclonic flows were found over several other guyots of the EC (Suiko, Nintoku and Koko) (Roden and Taft, 1985; Wagawa et al., 2012). We present on the distribution of methane above Koko and Jingu guyots (EC) and calculate CH_4 flux to the atmosphere for this region.

2. Material and methods

2.1. Water sampling and analysis

Water samples for the methane analysis were collected on cruise LV-86 aboard RV "Akademik M.A. Lavrentyev" (13–22 of July for Koko and 25–31 of July 2019 for Jingu guyots). We collected 200 samples of seawater for methane analysis at 25 stations. Hydrocasts were performed using a Rosette equipped with 8 5-L Niskin bottles and a CTD-system (SBE 19plus V2 SeaCAT, USA). All stations were occupied at night. Seawater was sampled using a silicone tube inserted into the bottom of pre-sterilized 68 ml glass vials and filling to overflow twice the volume. Immediately after filling, the vials were then tightly sealed with sterilized butyl rubber septum stopper with a needle for removing excess water.

A 12 ml headspace of ultra-pure helium (6.0 grade, Russian Federation) was introduced to a water sample from a dual-valve Tedlar Bag (Sigma-Aldrich, USA) through a needle by displacement of an equivalent amount of water. Then, the vials were shaken on a LS-110 shaker (LOIP, Russian Federation) for 4 h. Gas chromatography (GC) analyses were completed onboard the same day of sample collection. For GC analysis a "CrystalLux-4000M" (Meta-chrom, Russian Federation) gas chromatograph equipped with Hayesep R (80/100 mesh, 3 m) and Na-X (0.16–0.25 mm, 3 m) GC columns, flame ionization detector (FID) and two thermal conductivity detectors (TCD) was used. The aliquot of gas phase (6 ml) was injected into a GC sample loop (1 ml). Ultra-pure helium was used as a carrier gas. The analytical precision was 5%. The analytical error of methane analysis was 0.1 nM. The certified calibration gas mixtures (PGS-Service LLC, Russian Federation) with volumetric methane concentrations in helium of 10, 50 and 100 ppmv were used to calibrate the device.

Dissolved methane concentrations were measured using the headspace equilibration method described previously (Vereshchagina et al., 2013). The concentrations of dissolved methane were calculated according to the formula: $C_{water} = C_{gas}\ (K + V_{gas}/V_{water})$, where C_{water} is the methane concentration in a seawater sample, K is the partition or distribution coefficient for CH_4 in seawater, C_{gas} is the methane concentration in a gas phase determined via GC analysis, V_{gas} is the gas sample volume and V_{water} is the water sample volume. The K coefficient is determined according to formula $K = \beta RT/22.356$, where β is the Bunzen solubility coefficient for methane, T is a temperature, R is the gas constant and 22.356 is the molar volume of methane (Johnson et al., 1990). The results were corrected for the amount of CH_4 still dissolved in solution with Bunsen solubility coefficients (Wiesenburg and Guinasso, 1979) calculated from room temperature at the time of analysis and sample salinity.

2.2. Seawater-air methane flux calculation

The air-sea methane flux was calculated according to the flux equation $F=K(C^m-C^e)$, where K_m is a gas transfer coefficient (Cm h^{-1}), C^m is a measured methane concentration in seawater and C^e is an equilibrated seawater-air methane concentration. Gas transfer coefficient K is determined according to the formula (Wanninkhof, 2014) $K = 0.251<U^2>(Sc/660)^{-0.5}$, where U (m s^{-1}) is the average neutral stability of wind at 10 m height squared, and Sc is a Schmidt number. The Schmidt number for methane in a seawater is calculated as $Sc = 2101.2–131.54t+4.4931t^2-0.08676t^3+0.00070663t^4$, where t (C) is the water temperature (Wanninkhof, 2014). Wind speed was determined using the shipboard anemometer. The air CH_4 concentration was measured for each station. The resulting CH_4 flux was expressed in μmol m^{-2} d^{-1}.

3. Results and discussion

3.1. Koko guyot: CH_4 distribution in the water column and seawater-atmosphere CH_4 exchange

Koko (35°15′N 171°35′E) is located in the southern end of the EC. The seamount is a large shallow guyot with a flat top, reaching 230 m (Davies et al., 1972). The elliptical summit area (1935 km^2 at 365 m) is aligned in a northwest to southeast direction. Koko guyot has a thick carbonate cap. Koko and other guyots of the EC are of volcanic origin and are produced by the Hawaiian hotspot (Clague and Dalrymple, 1973). The southern part of EC lies in the North Pacific Transition Zone and is affected by Kuroshio Extension (KE).

Two sections across the summit of Koko guyot consisted of 16 CTD-stations (Fig. 1). The CH_4 concentration for section I varied from 1.4 to 6.5 nM, with an average of 4.3 nM. Its maximum content was associated with the bottom layers at 340 m at station 8. For the other stations 4, 6, 7, 9, 11 (266–361 m depth) a concentration of dissolved CH_4 (4.7 nM) was detected throughout the water column. Methane distributions from stations 4, 6, 7, 8, 9, 11 revealed no CH_4 maximum (Fig. 2A), representing a well-mixed water column above the summit. Deeper stations on the slopes of the guyot demonstrated similar trends of methane distribution. (Fig. 2B). The CH_4 concentration was almost constant (4.5–5.5 nM) throughout the water column at station 3, but at station 2 concentrations decreased slightly from 4.1 to 3.3 nM below 550 m. Another type of CH_4 distribution was observed in the deepest part of section I (Fig. 2C). For stations 1 and 13, methane was greatest (3.9–5 nM) in the upper 10–300 m. At these stations the minimal CH_4 concentrations (1.6–4 nM) were found from the bottom to about 500 m, a CH_4 distribution typical for open water (Reeburgh, 2007).

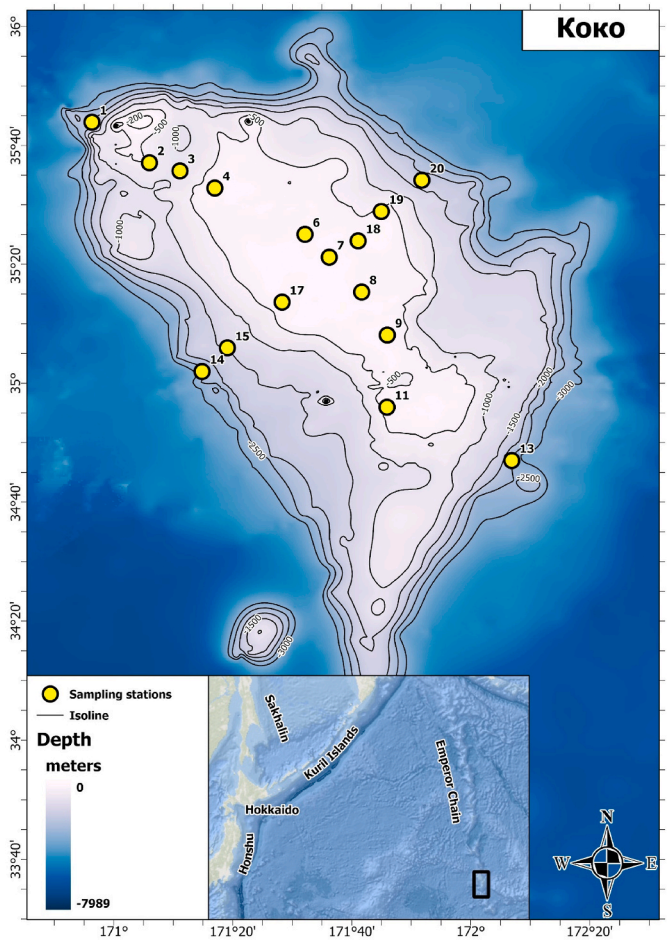

Fig. 1. Map of sampling locations, Koko guyot, Emperor Chain: Profile I (stations 1, 2, 3, 4, 6, 7, 8, 9, 11, 13); Profile II (stations 14, 15, 17, 7, 18, 19, 20).

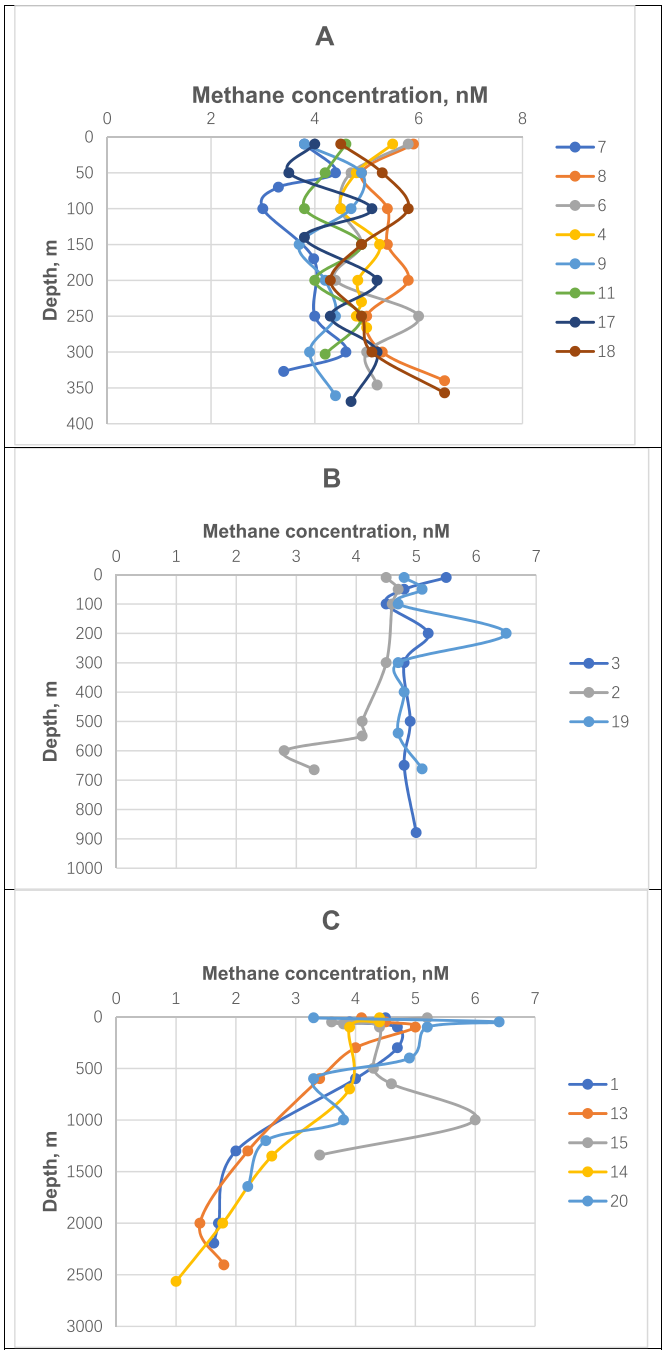

Fig. 2. Distribution of dissolved methane at the shallow A), mid-depth B) and deep-water C) stations.

Dissolved methane concentrations in section II ranged from 1 to 6.5 nM with a mean of 4.4 nM. For the shallow part of section a CH_4 maximum (6.4–6.5 nM) was observed at 357 m at station 18 and in a subsurface layer (200 m) at station 19. Another methane plume (6 nM) was also revealed at 1000 m in the deepest part of section II (station 15). The presence of the CH_4 plume at 500 m was unusual and may be considered a result of hydrodynamic conditions of water masses on the flanks of the guyots (Roden et al., 1982). Section I and II also clearly show the patchiness of CH_4 distribution (Fig. 3). Indeed, the methane maximum was associated mainly with the subsurface layers over the summit and eastern slope of the guyot. For the western slope of the guyot

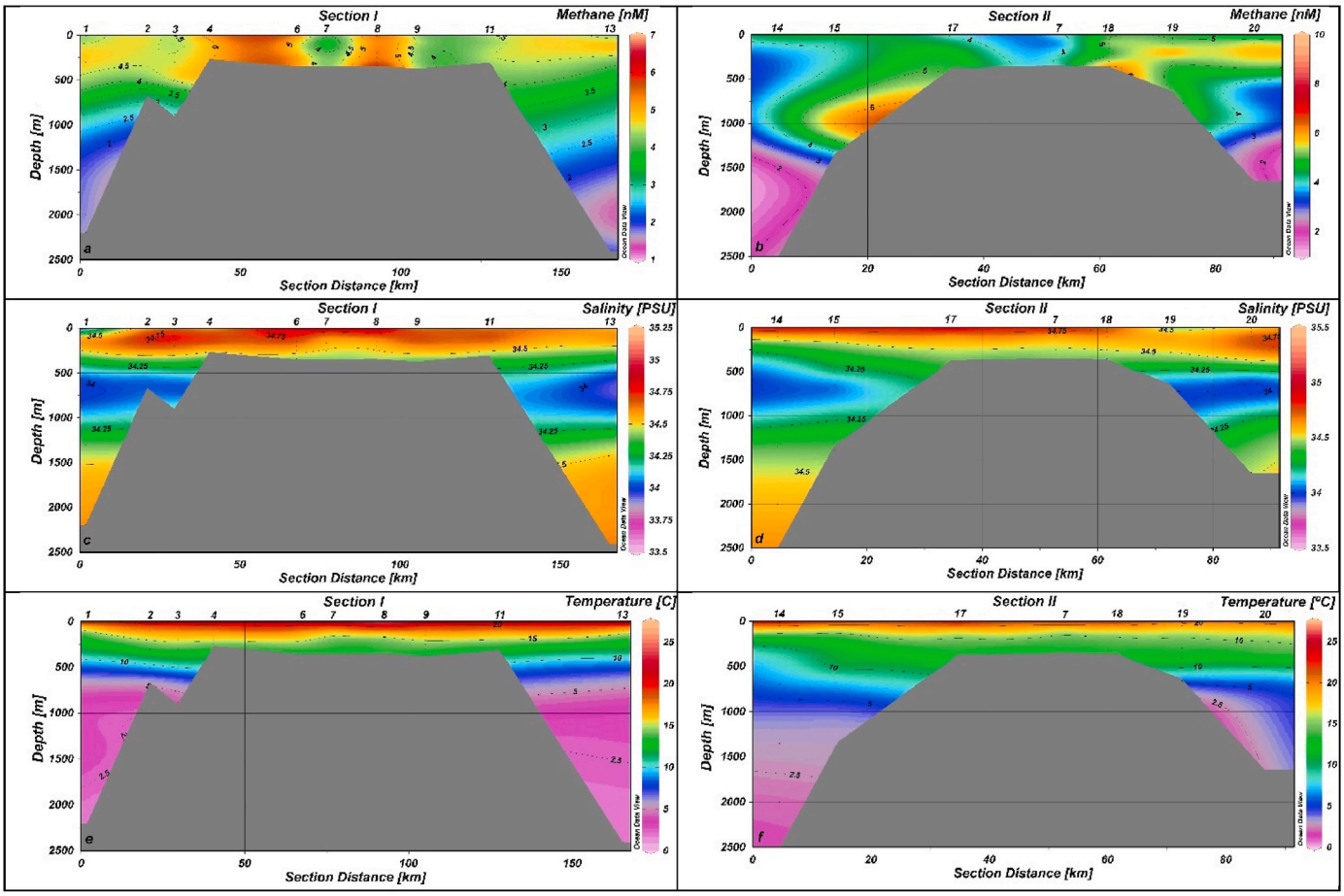

Fig. 3. Distribution of dissolved methane, salinity and temperature in the water column for Koko guyot: a) CH_4 in section I, b) CH_4 in section II, c) S in section I, d) S in section II, e) T in section I, f) T in section II.

the CH_4 maximum was "pushed" down likely by the action of the Kuroshio Extension (Roden et al., 1982). The difference in the pycnocline and other hydrological parameters were detected previously for the eastern and western slopes of Koko and other guyots of the Emperor Chain (Vastano et al., 1985; Roden and Taft, 1985).

The deepest stations 14 and 20 demonstrated the greatest variability in CH_4 content (Fig. 2C). The greatest methane concentrations (3.3–6.4 nM) were detected from 10 to 100 m. With increasing depth, the CH_4 content decreased monotonically to 1 nM at the deepest (2564 m) part of the section. Generally, the main features of methane distribution determined from section I and II were similar (Fig. 3a and b). The water column in the shallow parts of sections (10–357 m) contained greatest (3.5–6.5 nM) methane concentrations. However, the CH_4 content remained relatively high (3–5 nM) through 800 m. Such high values of CH_4 concentration below the surface mixed layer are not typical for open waters. Indeed, the measured background CH_4 content in the upper 300 m usually ranges from 2.2 to 3 nM (Watanabe et al., 1995).

An atmospheric equilibrium CH_4 concentration for both sections varied from 2.14 to 2.27 nM, averaging 2.19 nM (Table 1). Our data show that the surface water was supersaturated with respect to atmospheric CH_4 at all stations and acted as a source of methane for the atmosphere. The degree of oversaturation for surface water ranged from 8 to 52% (mean 32%) and is consistent with the average values (31%) previously defined in the open ocean surface waters for the northwestern Pacific (Watanabe et al., 1995). The greatest surface water supersaturation (30–52%) was found at shallow stations. Methane saturation followed the same trends as CH_4 concentrations in the upper part of the water column. The CH_4 oversaturation in the subsurface layers (10–300 m) was up to 2–3 times higher than the equilibrium methane concentration, which has been observed previously in various regions of the Pacific (Watanabe et al., 1995; Holmes et al., 2000; Kelley and Jeffrey, 2002) and Atlantic Oceans (Kolomijeca et al., 2022), as well as on the continental slope of the northeastern Pacific (Lapham et al., 2017). Surprisingly, the CH_4 oversaturation was also detected for the deeper part of section I and II to 1350 m. Undersaturated water were found only in the deepest (from 1350 to 2570 m) parts of the sections. The presence of water oversaturated with methane below 300 m was unusual and requires a more detailed discussion about the origin and possible sources of methane above the Emperor Chain.

It is unlikely that sediments are the primary source of CH_4 for the EC. Recent studies of sedimentary material from Koko guyot revealed elevated $CaCO_3$ and low total organic carbon content (Chen et al., 2021). These sediments were dominated by clay-silt and mainly affected by aeolian dust and could not generate a significant amount of methane. This was confirmed by the absence of a pronounced CH_4 maximum in the near-bottom water layers. As a result, the methane concentration for the shallow-water stations remained almost constant throughout the water column (Fig. 2A).

In situ biogenic CH_4 production is a more reasonable source of methane above the seamount. The proposed biogenic pathways of methane synthesis (Reeburgh, 2007; Bižić et al., 2020a) are controlled by oceanographic factors (salinity, temperature, pH, water movement, etc.). Several biogenic mechanisms of CH_4 formation occur in oligotrophic ocean waters. One is based on methanogenesis in anoxic microenvironments, such as suspended particles (Holmes et al., 2000; Sansone et al., 2001), faecal pellets (Cynar and Yayanos, 1991; Bianchi et al., 1992; Ditchfield et al., 2012) and guts of zooplankton (Schmale et al., 2018). Another proposed mechanism is the biodegradation of various

Table 1
Data of methane emission to the atmosphere and CH_4 content in surface layer, Koko seamount.

Station	Coordinates	T (C°)	S (‰)	Wind speed U (m/s)	CH_4^m (nM)	CH_4^{eq} (nM)	Oversaturation (%)	CH_4 air (ppm)	Flux density F (μmol m^{-2} day^{-1})
1	35°43.914 N 170°56.33 E	20.25	33.8	5	2.5	2.27	10	1.86	1.4
2	35°37.089 N 171°05.982 E	21.48	34.47	6	2.6	2.24	15	1.89	3.2
3	35°35.722 N 171°11.127 E	22.26	34.6	5	2.5	2.17	15	1.86	2.1
4	35°32.809 N 171°17.004E	22.65	34.42	7	3	2.2	36	1.9	10.2
6	35°25.030 N 171°32.132 E	22.58	34.77	7	2.9	2.22	30	1.92	8.6
7	35°21.190 N 171°36.217 E	24.5	34.98	8	2.9	2.14	35	1.92	13.2
8	34°14.110 N 171°41.972 E	24.02	34.89	7	3.1	2.16	43	1.92	12.4
9	35°08.083 N 171°45.98 E	23.49	34.5	8	3	2.17	37	1.91	14.2
11	34°55.983 N 171°45.945 E	22.78	34.51	7	3.3	2.19	50	1.9	14
13	34°46.982N 172°06.915 E	23.28	34.47	5	2.6	2.15	20	1.88	2.9
14	35°01.972 N 171°14.848 E	24.4	34.94	6	3.1	2.19	41	1.96	8.9
15	35°05.922 N 171°19.089 E	24.41	34.95	4	3.2	2.16	47	1.94	4.5
17	35°14.09 N 171°28.035 E	24.12	35	8	3.1	2.15	43	1.92	16.3
18	35°23.936 N 171°41.087 E	23	34.69	7	3.3	2.16	52	1.88	14.7
19	35°28.884 N 171°44.976 E	21.7	34.3	6	2.8	2.24	24	1.9	5
20	35°34.128 N 171°51.796 E	22.28	34.38	7	2.4	2.2	8	1.89	2.4
Mean		22.95	34.6	6.43	2.9	2.18	32	1.9	8.37

methylated organic substrates: utilization of methylphosphonates (MPn) (Karl et al., 2008) by MPn-utilizing bacteria and cyanobacteria (*Vibrio* and *Trichodesmium*; Ye et al., 2020), and cleavage of dimethylsulfoniopropionate (Damm et al., 2010) and subsequent demethylation of dimethylsulfide (Florez-Leiva et al., 2013) by methylotrophic microorganisms. Recent studies have shown that cyanobacteria (Bižić et al., 2020b) and marine algae (Klintzsch et al., 2019, 2023) produced CH_4 directly in the absence of methylphosphonates or other methylated substrates. All of these biogenic routes could occur above Koko. Further investigations are required to establish the contribution of each biogenic pathway to methane formation.

The upper mixed layer had temperatures up to 24°C with a sharp thermocline at a depth of 40–50 m. Below the thermocline the temperature decreased monotonically to a 1.69°C at the deepest (2570 m) station (Fig. 3e and f.). The salinity of the subsurface layer was relatively high and varied from 34.57 to 34.98 in the upper 100 m. A salinity maximum was detected at 10–50 m. Below upper 100 m salinity decreased until reaching a minimum of 34 at 500–650 m. The main core of the salinity minimum represented the influence of the North Pacific Intermediate Water (NPIW; You, 2003), which is transported from the Okhotsk Sea by cabelling along the subarctic-tropical frontal zone. Below 650 m the salinity increased gradually to 34.48–34.64 in the near-bottom layer at a deepest part of section I and II. The Koko guyot limited the flow of seawater to the east below the upper 500 m, which is apparent from the salinity sections for the NPIW and lower layers (Fig. 3c and d.). The weak uplift of isohalines and isotherms previously observed (Roden and Taft, 1985; Roden et al., 1982) for the western and eastern slopes of various guyots of the EC were also identified.

The surface layer was supersaturated (32%) throughout the study area (Table 1). These data agree well with the supersaturation level (31%) in the surface seawater at the section along 165°E from 34 to 40°N (Watanabe et al., 1995). However, another unexpected observation at Koko guyot was the detection of oversaturated seawater below 300 m, especially on the western slope of the seamount. The high methane content and supersaturation may have been caused by the several processes. First, the hydrological conditions could affect the CH_4 maxima distribution. As mentioned, the western slope of the guyot was affected by Kuroshio Extension (Roden et al., 1982). The KE is a continuation of the Kuroshio current after its separation from the Japanese coast at 36°N, 141°E. It is an eastward-flowing inertial jet crossing the Shatsky Rise and reaches the southern part of the EC (Vastano et al., 1985). The intrusion of undiluted Kuroshio water with a salinity greater than 34.6 (Roden and Taft, 1985) was detected at the western stations 11, 15, 17 from 10 to 150 m and could transfer the methane maximum from the upper part of the water column to 1000 m. A second factor that could influence the transfer of the CH_4 maximum were eddies that had been previously observed at 1000 m near the guyots of the EC (Wagawa et al., 2012). The increased methane saturation below 300 m may also be result from an export of dissolved (DOC) organic carbon by the NPIW to the intermediate waters over the EC (Hansell et al., 2002). Since the suspended particles and DOC are one of the major CH_4 sources for the oligotrophic Pacific Ocean (Holmes et al., 2000; Sansone et al., 2001), further investigations are necessary to understand the seamount influence on their distributions.

If the "seamount effect" could enhance *in situ* methane production and raise the CH_4 saturation level above the summit and on the slopes of the guyot, then the increased sea-air CH_4 emission should be detected at the surface. To confirm this hypothesis, we measured the sea-air CH_4 flux. The estimated sea-air CH_4 flux was high and ranged between 1.4 and 16.3 μmol m^{-2} day^{-1}, with an average of 8.37 μmol m^{-2} day^{-1} (Table 1). The average flux was 8.2 and 8.6 μmol m^{-2} day^{-1} for section I and II, respectively. The greatest sea-air methane flux (>10 μmol m^{-2} day^{-1}) was associated with the shallow water stations (4, 7, 8, 9, 17, 18) above the summit of the guyot and the deep station (11) on the southern slope. These values were significantly greater than previously estimated fluxes for open (0.2–0.3 μmol m^{-2} day^{-1}) and coastal oceans (1–2 μmol

m^{-2} day^{-1}) (Rhee et al., 2009) or recent studies based on the machine learning model for the Pacific Ocean Basin (0.33–0.94 μmol m^{-2} day^{-1}, reported as 0.65 to 1.84 Tg yr^{-1}; Weber et al., 2019). The increased flux could also be affected by meteorological conditions during the measurements. High wind speeds (>5 m/s) were measured at stations 4, 7, 8, 9, 11, 17, and 18 that had the greatest sea-air CH_4 fluxes. Nevertheless, the fluxes at stations 1, 3, 13, 15 with a low wind speed (≤5 m/s) were high (from 1.4 to 4.5 μmol m^{-2} day^{-1}) as well. Another factor that could influence the air-sea methane exchange at Koko guyot was a typhoon passing just before our measurements. Typhoons and storms accelerate the temporal and local CH_4 emission by mixing of the upper layers and increasing air-sea exchanges (Vereshchagina et al., 2013; Vetrov et al., 2018). For Koko, high wind speeds occurred at the most stations.

3.2. *Jingu guyot: CH_4 distribution in the water column and seawater-atmosphere CH_4 exchange*

Jingu Seamount (38°47′N 171°11′E) is located about 675 km north of the Hawaiian–Emperor bend in the Main Gap of the Emperor Seamount chain near Ojin. It is a relatively small (summit area about 450 km^2) and deep guyot with the summit at a water depth of 850 m. Two short sections III and IV of nine CTD-stations were positioned over the summit of Jingu guyot (Fig. 4). CH_4 concentrations varied from 1.4 to 6 nM, averaging 3.5 nM. The greatest methane concentration (6 nM) was found at 10 m at station 24 and the lowest in the deepest part of section III below 2000 m. The general pattern of methane distribution was similar for sections III and IV (Fig. 5a and b). The greatest CH_4 concentration (3.8–6 nM) was associated with the upper water column

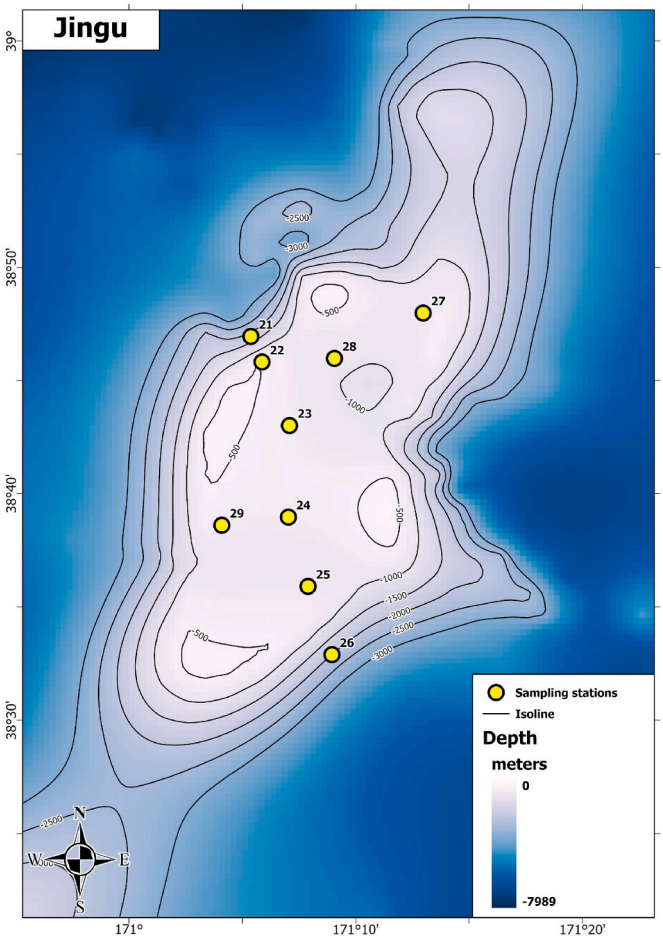

Fig. 4. Map of sampling locations, Jingu guyot, Emperor Chain: Section III (stations 21, 22, 23, 24, 25, 26); Section IV (stations 27, 28, 23, 29).

(10–300 m). Below 400 m the methane decreased to 1.4–1.8 nM for the deep-water stations (29, 21) and to 1.8–2.7 nM for stations 23, 27, 28, and 29 located above the summit. Generally, the patterns of methane distribution for Jingu were more typical of the open ocean (Watanabe et al., 1995).

Atmospheric equilibrium concentration over the summit of Jingu varied from 2.38 to 2.47 nM (mean 2.42 nM; Table 2). The surface layer was supersaturated with respect to atmospheric CH_4 for all stations. The average degree of oversaturation (20%) was lower than the values previously found (32 %) for the surface seawater above Koko seamount. There were no differences of CH_4 saturation for the surface layers between the shallow and deep-water stations, unlike at Koko guyot. Nevertheless, CH_4 oversaturations were observed in the deeper parts of sections III and IV through 750 m.

The subsurface layer temperature of the water column above Jingu ranged from 16.26 to 20.14°C with a sharp thermocline at 50 m. Below the upper 100 m the temperature decreased monotonically to 1.8°C near the bottom (Fig. 5e and f). The salinity maximum (34.63) was also found between 10 and 50 m. The core of salinity minimum (33.94) was associated with the layer of North Pacific Intermediate water (500 m), as it was for Koko guyot. Under the NPIW, the salinity increased to 34.6 at the bottom, as the Jingu guyot did not block the transport of the NPIW like the Koko guyot (Fig. 5c and d).

The estimated sea-air CH_4 flux for Jingu guyot ranged from 0.5 to 6.5 μmol m^{-2} day^{-1}, with an average of 2.6 μmol m^{-2} day^{-1} (Table 2). The average flux for Jingu was three times lower than that for Koko (8.37 μmol m^{-2} day^{-1}). The fluxes for Jingu (0.5–6.5 μmol m^{-2} day^{-1}) were comparable with the fluxes for Koko (1.4–4.5 μmol m^{-2} day^{-1}) only at stations 1, 2, and 3 that had low wind speeds (≤5 m/s). A decreased flux for Jingu was caused by the lower average wind speed (4.55 m/s) and lower temperature of the surface layer (18.84°C), because the solubility of methane in seawater increases at low temperatures. Nevertheless, the average flux for Jingu was from 1.3 to 2.6 times higher than the average flux for the coastal ocean (Rhee et al., 2009). However, these flux values are not unique to the Pacific Ocean; the mean June air-sea methane exchange for the Eastern Tropical North Pacific is 2.3 ± 0.9 μmol m^{-2} day^{-1} (Sansone et al., 2001). The flux varied from 1.4 to 1.7 μmol m^{-2} day^{-1} for station ALOHA near the Hawaiian Islands (Holmes et al., 2000) and from 0.9 to 3.5 μmol m^{-2} day^{-1} northwest of station ALOHA (Tilbrook and Karl, 1995). The CH_4 flux was also estimated for other parts of Pacific: the air-sea exchange of CH_4 for a transect in the southern hemisphere ranged from −0.74 ± 0.73 to 4.13 ± 1.01 μmol m^{-2} day^{-1} (Kelley and Jeffrey, 2002). For the marginal seas (East China Sea) the flux was higher (6.5–7.4 μmol m^{-2} day^{-1}) than for the open ocean (Ye et al., 2016). As methane fluxes vary spatially, temporarily and locally, we suggest that the average methane fluxes for Koko and Jingu guyots (8.37 and 2.6 μmol m^{-2} day^{-1}) are consistent with the published exchange data for the Pacific Ocean.

4. Conclusions

Seamounts were not previously considered as important regions for methane production. We presented results on CH_4 distributions and estimated the ocean-atmosphere CH_4 flux for two gyuots (Koko and Jingu) in the southern portion of the Emperor Chain. Our results revealed that the methane concentrations (3.9–6.5 nM) in the upper part of the water column above the summits was at least two times higher than the CH_4 content (2.2–3 nM) previously found in the open Pacific Ocean. The methane maxima for Koko (3.9–6.5 nM) and Jingu (3.8–6 nM) were found in the subsurface or near bottom layers over the seamount summit. The methane distribution for Koko and Jingu was different, with the methane maximum (6 nM) on the western slope of Koko found at 1000 m. This was caused by the action of the Kuroshio Extension or a deep eddy. The methane maxima (3.8–6 nM) were detected only in the upper part of the water column over the Jingu summit.

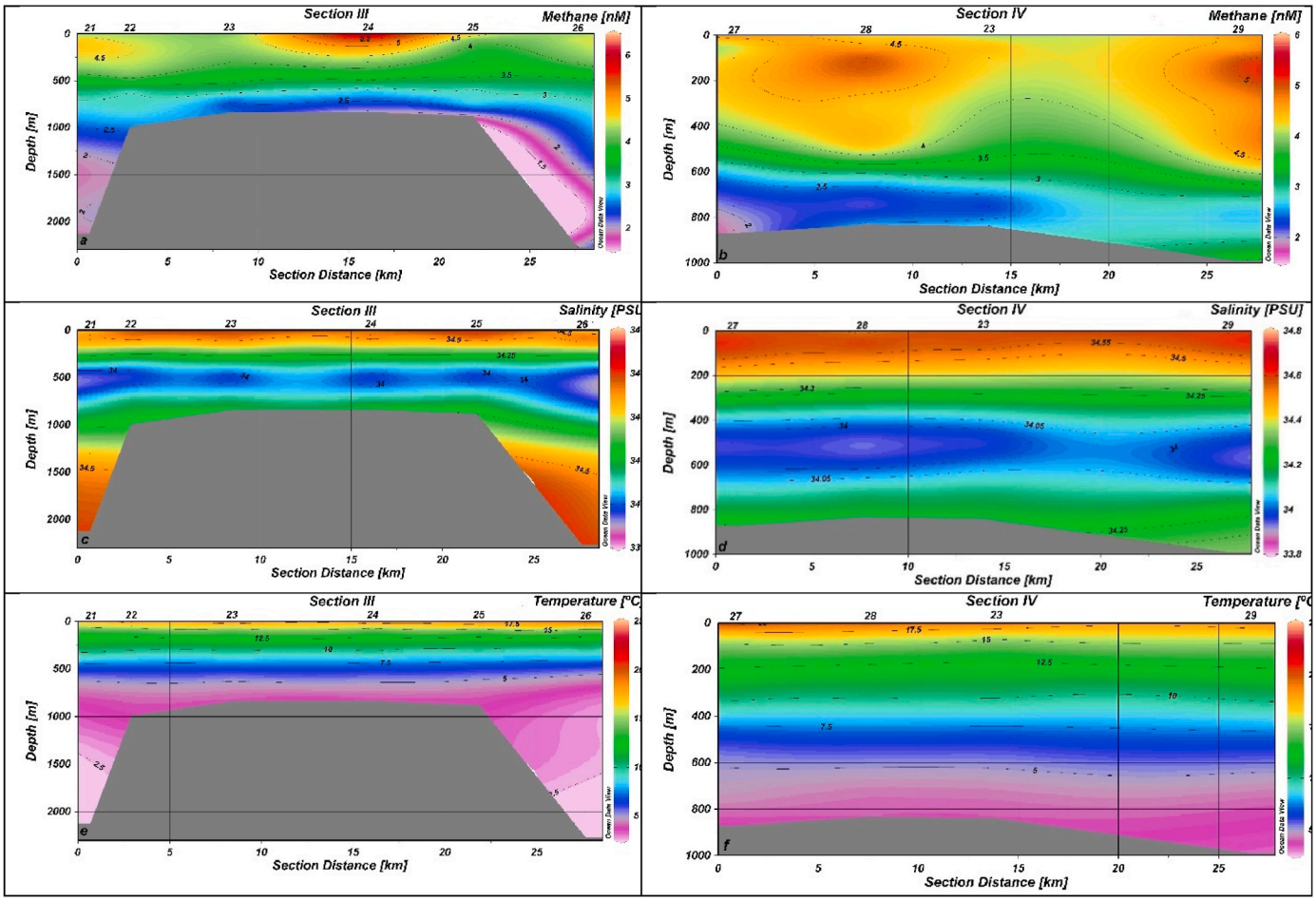

Fig. 5. Distribution of dissolved methane, salinity and temperature in the water column for Jingu guyot: a) CH_4 in section III, b) CH_4 in section IV, c) S in section III d) S in section IV e) T in section III f) T in section IV.

Table 2
Data of methane emission to the atmosphere and CH_4 content in surface layer, Jingu seamount.

Station	Coordinates	Water temperature (C°)	Salinity (‰)	Wind speed U (m/s)	Measured CH_4^m (nM)	Equilibrated CH_4^{eq} (nM)	Oversaturation (%)	CH_4 air (ppm)	Flux density F (μmol m^{-2} day^{-1})
21	38° 46.944 N 171° 05.378E	17.16	34.44	6	3.10	2.47	25	1.91	5.1
22	38° 45.813 N 171° 05.872 E	18.35	34.53	5	3.30	2.46	33	1.95	4.9
23	38° 43.014 N 171° 07.088 E	18.99	34.56	7	2.90	2.34	23	1.88	6.5
24	38° 38.967 N 171° 07.033 E	18.97	34.49	4	2.80	2.44	14	1.96	1.3
25	38° 35.902 N 171° 07.901 E	19.61	34.57	3	3.20	2.41	32	1.96	1.7
26	38° 32.891 N 171° 08.951 E	20.14	34.37	5	3.00	2.39	25	1.96	3.7
27	38° 47.983 N 171°12.981 E	18.75	34.56	3	2.70	2.38	13	1.96	0.7
28	38° 45.976 N 171°09.062 E	19.32	34.63	4	2.70	2.43	10	1.97	1
29	38° 36.945 N 171°02.925 E	18.31	34.63	4	2.60	2.46	5	1.95	0.5
Mean		18.84	34.53	4.55	2.92	2.42	20	1.94	2.6

The surface water layer was supersaturated with respect to atmospheric CH_4 for both seamounts and acted as a source of methane to the atmosphere. The seawater supersaturated with CH_4 was also detected in the subsurface (10–300 m) and below the upper 300 m in parts of water column. The previously described "seamount effect" could influence the distribution of anoxic niches (suspended particles and zooplankton) and methane producing bacteria, cyanobacteria and algae over the summit and in the vicinity of the guyots which may have led to increased methane production. Our suggestion was supported by the high methane fluxes over the Koko and Jingu guyots. The estimated average methane flux for Koko (8.37 μmol m^{-2} day^{-1}) and Jingu (2.8 μmol m^{-2} day^{-1}) was several times higher than the flux for open and coastal ocean waters and was caused by high wind speeds. If the "seamount effect" could enhance methanogenesis over the summits of guyots, then the impact the seamounts on the global CH_4 emission is higher than previously considered, suggesting that further studies of methanogenesis over seamounts necessary to better understand the reasons for the increased methane production.

CRediT authorship contribution statement

Nikita S. Polonik: Writing – original draft, Methodology, Investigation, Formal analysis. **Alexey A. Legkodimov:** Writing – original draft, Visualization, Resources, Investigation.

Declaration of competing interest

The authors declare that they have no known competing financial interests or personal relationships that could have appeared to influence the work reported in this paper.

Acknowledgments

This work was supported by the State Assignment of POI FEB RAS FWMM-2024-0029. We are grateful to the captain (Victor B. Ptushkin) and crew of the RV Akademik M.A. Lavrentyev for their help in sampling. We appreciate Dr. Oleg. G. Borzykh and Mr. Alexei M. Koltunov for their technical assistance, Dr. Tatiana N. Dautova and the Direction of NSCMB FEB RAS for the invitation to take part in the cruise. Alexei A. Legkodimov expresses special respect to an agent A. Bird for his help with a sea winch.

Data availability

Data will be made available on request.

References

Archer, D., Buffett, B., Brovkin, V., 2009. Ocean methane hydrates as a slow tipping point in the global carbon cycle. Proc. Natl. Acad. Sci. U.S.A. 106 (49), 20596–20601. https://doi.org/10.1073/pnas.0800885105.

Bianchi, M., Marty, D., Teyssie, J.L., Fowler, S.W., 1992. Strictly aerobic and anaerobic bacteria associated with sinking particulate matter and zooplankton fecal pellets. Mar. Ecol.: Prog. Ser. 88, 55–60. https://doi.org/10.3354/meps088055.

Bižić, M., Grossart, H.-P., Ionescu, D., 2020a. Methane paradox. In: eLS. John Wiley & Sons, Ltd, Chichester. https://doi.org/10.1002/9780470015902.a0028892.

Bižić, M., Klintzsch, T., Ionescu, D., Hindiyeh, M.Y., Günthel, M., Muro-Pastor, A.M., Eckert, W., Urich, T., Keppler, F., Grossart, H.-P., 2020b. Aquatic and terrestrial cyanobacteria produce methane. Sci. Adv. 6 (3), eaax5343. https://doi.org/10.1126/sciadv.aax5343.

Boehlert, G.W., 1988. Current-topography interactions at mid-ocean seamounts and the impact on pelagic ecosystems. Geojournal 16 (1), 45–52. https://doi.org/10.1007/BF0262637.

Bogard, M.J., del Giorgio, P.A., Boutet, L., Chaves, M.C.G., Prairie, Y.T., Merante, A., Derry, A.M., 2014. Oxic water column methanogenesis as a major component of aquatic CH_4 fluxes. Nat. Commun. 5, 5350. https://doi.org/10.1038/ncomms6350.

Bograd, S.J., Rabinovich, A.B., Le Blond, P.H., Shore, J.A., 1997. Observations of seamount-attached eddies in the North Pacific. J. Geophys. Res.: Oceans 102 (C6), 12441–12456. https://doi.org/10.1029/97/JC00585.

Busch, K., Hanz, U., Mienis, F., Mueller, B., Franke, A., Roberts, E.M., Rapp, H.T., Hentschel, U., 2020. On giant shoulders: how a seamount affects the microbial community composition of seawater and sponges. Biogeosciences 17, 3471–3486. https://doi.org/10.5194/bg-17-3471-2020.

Canadell, J.G., Monteiro, P.M.S., Costa, M.H., Cotrim da Cunha, L., Cox, P.M., Eliseev, A. V., Henson, S., Ishii, M., Jaccard, S., Koven, C., Lohila, A., Patra, P.K., Piao, S., Rogelj, J., Syampungani, S., Zaehle, S., Zickfeld, K., 2021. Global carbon and other biogeochemical cycles and feedbacks. In: Masson-Delmotte, V., Zhai, P., Pirani, A., Connors, S.L., Péan, C., Berger, S., Caud, N., Chen, Y., Goldfarb, L., Gomis, M.I., Huang, M., Leitzell, K., Lonnoy, E., Matthews, J.B.R., Maycock, T.K., Waterfield, T., Yelekçi, O., Yu, R., Zhou, B. (Eds.), Climate Change 2021: the Physical Science Basis. Contribution of Working Group I to the Sixth Assessment Report of the Intergovernmental Panel on Climate Change. Cambridge University Press, Cambridge, United Kingdom and New York, NY, USA, pp. 673–816. https://doi.org/10.1017/9781009157896.007.

Clague, D.A., Dalrymple, G.B., 1973. Age of kōko seamount, emperor seamount chain. Earth Planet Sci. Lett. 17 (2), 411–415. https://doi.org/10.1016/0012-821X(73)90209-4.

Clark, M.R., Watling, L., Rowden, A.A., Guinotte, L.M., Smith, C.R., 2011. A global seamount classification to aid the scientific design of marine protected area networks. Ocean Coast Manag. 54, 19–36. https://doi.org/10.1016/j.ocecoaman.2010.10.006.

Chen, J., Zou, J., Zhu, A., Shi, X., Nürnberg, D., Lembke-Jene, L., Tiedemann, R., Wang, K., Wu, Y., Dong, Z., Liu, J., Dou, R., 2021. Geochemistry of surface sediments from the emperor seamount chain, North Pacific. Front. Earth Sci. 9, 674842. https://doi.org/10.3389/feart.2021.674842.

Chronopoulou, P.-M., Shelley, F., Pritchard, W.J., Maanoja, S., Trimmer, M., 2017. Origin and fate of methane in the Eastern Tropical North Pacific oxygen minimum zone. ISME J. 11 (6), 1386–1399. https://doi.org/10.1038/ismej.2017.6.

Cynar, F.J., Yayanos, A.A., 1991. Enrichment and characterization of a methanogenic bacterium from the oxic upper layer of the ocean. Curr. Microbiol. 23 (2), 89–96. https://doi.org/10.1007/BF02092256.

Dai, S., Zhao, Y., Li, X., Wang, Z., Zhu, M., Liang, J., Liu, H., Sun, X., 2020. The seamount effect on phytoplankton in the tropical western Pacific. Mar. Environ. Res. 162, 105094. https://doi.org/10.1016/j.marenvres.2020.105094.

Dai, S., Zhao, Y., Li, X., Wang, Z., Zhu, M., Liang, J., Liu, H., Sun, X., 2022. Seamount effect on phytoplankton biomass and community above a deep seamount in the tropical western Pacific. Mar. Pollut. Bull. 175, 113354. https://doi.org/10.1016/j.marpolbul.2022.113354.

Damm, E., Helmke, E., Thoms, S., Schauer, U., Nöthig, E., Bakker, K., Kiene, R.P., 2010. Methane production in aerobic oligotrophic surface water in the central Arctic Ocean. Biogeosciences 7 (3), 1099–1108. https://doi.org/10.5194/bg-7-1099-2010.

Dautova, T.N., Galkin, S.V., Tabachnik, K.R., Minin, K.V., Kireev, P.A., Moskovtseva, A. V., Adrianov, A.V., 2019. The first data on the structure of vulnerable marine ecosystems of the Emperor Chain Seamounts: indicator taxa, landscapes, and biogeography. Russ. J. Mar. Biol. 45 (6), 408–417. https://doi.org/10.1134/S1063074019060026.

Davies, T.A., Wilde, P., Clague, D.A., 1972. Kōko Seamount: a major guyot at the southern end of the Emperor Seamounts. Mar. Geol. 13 (5), 311–321. https://doi.org/10.1016/0025-3227(72)90013-8.

Ditchfield, A.K., Wilson, S.T., Hart, M.C., Purdy, K.J., Green, D.H., Hatton, A.D., 2012. Identification of putative methylotrophic and hydrogenotrophic methanogens within sedimenting material and copepod faecal pellets. Aquat. Microb. Ecol. 67 (2), 151–160. https://doi.org/10.3354/ame01585.

Djurhuus, A., Read, J.F., Rogers, A.D., 2017. The spatial distribution of particulate organic carbon and microorganisms on seamounts of the South West Indian Ridge. Deep-Sea Res. II 136, 73–84. https://doi.org/10.1016/j.dsr2.2015.11.015.

Etiope, G., Schwietzke, S., 2019. Global geological methane emissions: an update of top-down and bottom-up estimates. Elem. Sci. Anth. 7, 47. https://doi.org/10.1525/elementa.383.

Ferry, J.G., Lessner, D.J., 2008. Methanogenesis in marine sediments. Ann. N. Y. Acad. Sci. 1125 (1), 147–157. https://doi.org/10.1196/annals.1419.007.

Florez-Leiva, L., Damm, E., Farías, L., 2013. Methane production induced by dimethylsulfide in surface water of an upwelling ecosystem. Prog. Oceanogr. 112–113, 38–48. https://doi.org/10.1016/j.pocean.2013.03.005.

Hamdan, L.J., Wickland, K.P., 2016. Methane emissions from oceans, coasts, and freshwater habitats: new perspectives and feedbacks on climate. Limnol. Oceanogr. 61 (S1), 3–12. https://doi.org/10.1002/lno.10449.

Hansell, D.A., Carlson, C.A., Suzuki, Y., 2002. Dissolved organic carbon export with North Pacific intermediate water formation. Global Biogeochem. Cycles 16 (1), 1007. https://doi.org/10.1029/2000GB001361.

Hiruta, A., Matsumoto, R., 2022. Massive gas hydrates buried on Umitaka Spur in the Sea of Japan: description, origin, and significance to methane cycling in marine sediment. Geo Mar. Lett. 42, 13. https://doi.org/10.1007/s00367-022-00735-w.

Holmes, M.E., Sansone, F.J., Rust, T.M., Popp, B.N., 2000. Methane production, consumption, and air-sea exchange in the open ocean: an evaluation based on carbon isotopic ratios. Global Biogeochem. Cycles 14 (1), 1–10. https://doi.org/10.1029/1999GB001209.

Jin, Y.K., Kim, Y.-G., Baranov, B., Shoji, H., Obzhirov, A., 2011. Distribution and expression of gas seeps in a gas hydrate province of the northeastern Sakhalin continental slope, Sea of Okhotsk. Mar. Petrol. Geol. 28 (10), 1844–1855. https://doi.org/10.1016/j.marpetgeo.2011.03.007.

Johnson, K.M., Hughes, J.E., Donaghay, P.L., Sieburth, J.McN., 1990. Bottle-calibration static head space method for the determination of methane dissolved in seawater. Anal. Chem. 62, 2408–2412. https://doi.org/10.1021/ac00220a030.

Karl, D.M., Beversdorf, L., Björkman, K.M., Church, M.J., Martinez, A., DeLong, E.F., 2008. Aerobic production of methane in the sea. Nat. Geosci. 1, 473–478. https://doi.org/10.1038/ngeo234.

Kelley, C.A., Jeffrey, W.H., 2002. Dissolved methane concentration profiles and air-sea fluxes from 41°S to 27°N. Global Biogeochem. Cycles 16 (3). https://doi.org/10.1029/2001GB001809, 13-1–13-6.
Kiriakoulakis, K., Wolff, G., 2005. Organic biogeochemistry of seamounts: a review. Oasis Report. http://epic.awi.de/id/eprint/37314/19/OASIS_Biogeochemistry.pdf.
Klintzsch, T., Langer, G., Nehrke, G., Wieland, A., Lenhart, K., Keppler, F., 2019. Methane production by three widespread marine phytoplankton species: release rates, precursor compounds, and potential relevance for the environment. Biogeosciences 16 (20), 4129–4144. https://doi.org/10.5194/bg-16-4129-2019.
Klintzsch, T., Geisinger, H., Wieland, A., Langer, G., Nehrke, G., Bizic, M., Greule, M., Lenhart, K., Borsch, C., Schroll, M., Keppler, F., 2023. Stable carbon isotope signature of methane released from phytoplankton. Geophys. Res. Lett. 50, e2023GL103317. https://doi.org/10.1029/2023GL103317.
Komaki, K., Kawabe, M., 2009. Deep-circulation current through the main Gap of the emperor seamounts chain in the North Pacific. Deep-Sea Res., Part A I. 56 (3), 305–313. https://doi.org/10.1016/j.dsr.2008.10.006.
Kolomijeca, A., Marx, L., Reynolds, S., Cariou, T., Mawji, E., Boulart, C., 2022. An update on dissolved methane distribution in the subtropical North Atlantic Ocean. Ocean Sci. 18, 1377–1388. https://doi.org/10.5194/os-18-1377-2022.
Kono, T., Kawasaki, Y., 1997. Results of CTD and mooring observations southeast of Hokkaido: Part 1. Annual velocity and transport variations in the Oyashio. Bull. Hokkaido Natl. Fish. Inst. 61, 65–81.
Kosmach, D.A., Sergienko, V.I., Dudarev, O.V., Kurilenko, A.V., Gustafsson, O., Semiletov, I.P., Shakhova, N.E., 2015. Methane in the surface waters of Northern Eurasian marginal seas. Dokl. Chem. 465 (2), 281–285. https://doi.org/10.1134/S0012500815120022.
Lan, X., Thoning, K.W., Dlugokencky, E.J., 2023. Trends in globally-averaged CH_4, N_2O, and SF_6 determined from NOAA global monitoring laboratory measurements. Version 2023-11. https://doi.org/10.15138/P8XG-AA10.
Lapham, L., Marshall, K., Magen, C., Lyubchich, V., Cooper, L.W., Grebmeier, J.M., 2017. Dissolved methane concentrations in the water column and surface sediments of hanna shoal and barrow canyon, northern chukchi sea. Deep-Sea Res. II 144, 92–103. https://doi.org/10.1016/j.dsr2.2017.01.004.
Ma, J., Song, J., Li, X., Wang, Q., Zhong, G., 2021. Multidisciplinary indicators for confirming the existence and ecological effects of a Taylor column in the Tropical Western Pacific Ocean. Ecol. Indicat. 127, 107777. https://doi.org/10.1016/j.ecolind.2021.107777.
Mao, S.-H., Zhang, H.-H., Zhuang, G.-C., Li, X.-J., Liu, Q., Zhou, Z., Wang, W.-L., Li, C.-Y., Lu, K.-Y., Liu, X.-T., Montgomery, A., Joye, S.B., Zhang, Y.-Z., Yang, G.-P., 2022. Aerobic oxidation of methane significantly reduces global diffusive methane emissions from shallow marine waters. Nat. Commun. 13, 7309. https://doi.org/10.1038/s41467-022-35082-y.
Mar, K.A., Unger, C., Walderdorff, L., Butler, T., 2022. Beyond CO_2 equivalence: the impacts of methane on climate, ecosystems, and health. Environ. Sci. Pol. 134, 127–136. https://doi.org/10.1016/j.envsci.2022.03.027.
Marsac, F., Annasawmy, P., Noyon, M., Demarcq, H., Soria, M., Rabearisoa, N., Bach, P., Cherel, Y., Grelet, J., Romanov, E., 2020. Seamount effect on circulation and distribution of ocean taxa in the vicinity of La Pérouse, a shallow seamount in the southwestern Indian Ocean. Deep-Sea Res. II 176 (23), 104806. https://doi.org/10.1016/j.dsr2.2020.104806.
Matveeva, T., Logvina, E., Nazarova, O., Gladysh, V., 2022. Gas hydrate-bearing province of Eastern Sakhalin slope (Sea of Okhotsk): geological setting and factor of control. In: Mienert, J., Berndt, C., Tréhu, A.M., Camerlenghi, A., Liu, C.S. (Eds.), World Atlas of Submarine Gas Hydrates in Continental Margins. Springer, Cham. https://doi.org/10.1007/978-3-030-81186-0_32.
Mendonça, A., Arístegui, J., Vilas, J.C., Montero, M.F., Ojeda, A., Espino, M., Martins, A., 2012. Is there a seamount effect on microbial community and biomass? The case study of Seine and Sedlo Seamounts (Northeast Atlantic). PLoS One 7 (1), e29526. https://doi.org/10.1371/journal.pone.0029526.
Ota, Y., Suzumura, M., Tsukasaki, A., Suzuki, A., Seike, K., Minatoya, J., 2022. Sediment accumulation rates and particle mixing at northwestern Pacific seamounts. J. Mar. Syst. 229, 103719. https://doi.org/10.1016/j.jmarsys.2022.103719.
Pack, M.A., Heintz, M.B., Reeburgh, W.S., Trumbore, S.E., Valentine, D.L., Xu, X., Druffel, E.R.M., 2015. Methane oxidation in the eastern tropical North Pacific Ocean water column. J. Geophys. Res. Biogeosci. 120 (6), 1078–1092. https://doi.org/10.1002/2014JG002900.
Reeburgh, W.S., 2007. Oceanic methane biogeochemistry. Chem. Rev. 107 (2), 486–513. https://doi.org/10.1021/cr050362v.
Rhee, T.S., Kettle, A.J., Andreae, M.O., 2009. Methane and nitrous oxide emissions from the ocean: a reassessment using basin-wide observations in the Atlantic. J. Geophys. Res. Atmos. 114 (D12304). https://doi.org/10.1029/2008JD011662.
Roden, G.I., Taft, B.A., Ebbesmeyer, C.C., 1982. Oceanographic aspects of the Emperor seamounts region. J. Geophys. Res. 87 (C12), 9537–9552. https://doi.org/10.1029/JC087iC12p09537.
Roden, G.I., Taft, B.A., 1985. Effect of the Emperor Seamounts on the mesoscale thermohaline structure during the summer of 1982. J. Geophys. Res. 90 (C1), 839–855. https://doi.org/10.1029/JC090iC01p00839.
Rogers, A.D., 2018. The biology of seamounts: 25 Years on. Adv. Mar. Biol. 79, 137–224. https://doi.org/10.1016/bs.amb.2018.06.001.
Sansone, F.J., Popp, B.N., Gasc, A., Graham, A.W., Rust, T.M., 2001. Highly elevated methane in the eastern tropical North Pacific and associated isotopically enriched fluxes to the atmosphere. Geophys. Res. Lett. 28 (24), 4567–4570. https://doi.org/10.1029/2001GL013460.
Schmale, O., Wäge, J., Mohrholz, V., Wasmund, N., Gräwe, U., Rehder, G., Labrenz, M., Loick-Wilde, N., 2018. The contribution of zooplankton to methane supersaturation in the oxygenated upper waters of the central Baltic Sea. Limnol. Oceanogr. 63 (1), 412–430. https://doi.org/10.1002/lno.10640, 412–430.
Sokolova, N.L., Telegin, YuA., Obzhirov, A.I., 2021. Methane flux and gas hydrate accumulations in the Sea of Okhotsk and their ecological aspects. Vietnam J. of Earth Sci. 43 (3), 273–284. https://doi.org/10.15625/2615-9783/16193.
Sun, M.-S., Zhang, G.-L., Cao, X.-P., Mao, X.-Y., Li, J., Ye, W.-W., 2015. Methane distribution, fluxes, and budget in the east China sea and yellow sea. Biogeosci. Discuss. 12 (9), 7017–7053. https://doi.org/10.5194/bgd-12-7017-2015.
Tilbrook, B.D., Karl, D.M., 1995. Methane sources, distributions and sinks from California coastal waters to the oligotrophic North Pacific gyre. Mar. Chem. 49 (1), 51–64. https://doi.org/10.1016/0304-4203(94)00058-L.
Toki, T., Chibana, H., Shimabukuro, T., Yamakawa, Y., 2023. Distribution of dissolved methane in seawater from the East China Sea to the Ryuku forearc. Front. Earth Sci. 11, 1174504. https://doi.org/10.3389/feart.2023.1174504.
Turnewitsch, R., Falahat, S., Nycander, J., Dale, A., Scott, R.B., Furnival, D., 2013. Deep-sea fluid and sediment dynamics–Influence of hill-to seamount-scale seafloor topography. Eart-Science Rev. 127, 203–241. https://doi.org/10.1016/j.earscirev.2013.10.005.
Turnewitsch, R., Dumont, M., Kiriakoulakis, K., Legg, S., Mohn, C., Peine, F., Wolff, G., 2016. Tidal influence on particulate organic carbon export fluxes around a tall seamount. Prog. Oceanogr. 149, 189–213. https://doi.org/10.1016/j.pocean.2016.10.009.
Van Amstel, A., 2012. Methane. A review. J. Integr. Environ. Sci. 9 (Suppl. 1), 5–30. https://doi.org/10.1080/1943815X.2012.694892.
Vastano, A.C., Hagan, D.E., McNally, G.J., 1985. Lagrangian observations of surface circulation at the Emperor Seamount Chain. J. Geophys. Res. 90 (C2), 3325–3331. https://doi.org/10.1029/JC090iC02p03325.
Vereshchagina, O.F., Korovitskaya, E.V., Mishukova, G.I., 2013. Methane in water columns and sediments of the north western Sea of Japan. Deep-Sea Res. II 86–87, 25–33. https://doi.org/10.1016/j.dsr2.2012.08.017.
Vetrov, A.A., Lobus, N.V., Drozdova, A.N., Belyaev, N.A., Romankevich, E.A., 2018. Methane in water and bottom sediments in three sections in the Kara and Laptev seas. Oceanology (Engl. Transl.) 58, 198–204. https://doi.org/10.1134/S0001437018020157.
Vilas, J.C., Arístegui, J., Kiriakoulakis, K., Wolff, G.A., Espino, M., Polo, I., Montero, M. F., Mendonça, A., 2009. Seamounts and organic matter–Is there an effect? The case of Sedlo and Seine Seamounts: Part 1. Disitributions of dissolved and particulate organic matter. Deep-Sea Res. II 56 (25), 2618–2630. https://doi.org/10.1016/j.dsr2.2008.12.023.
Wagawa, T., Yoshikawa, Y., Isoda, Y., Oka, E., Uehara, K., Nakano, T., Kuma, K., Takagi, S., 2012. Flow fields around the Emperor Seamounts detected from current data. J. Geophys. Res. 117, C06006. https://doi.org/10.1029/2011JC007530.
Wang, B., Doust, H., Liu, J., 2019. Geology and petroleum systems of the east China sea basin. Energies 12 (21), 4088. https://doi.org/10.3390/en12214088.
Wanninkhof, R., 2014. Relationship between wind speed and gas exchange over the ocean revisited. Limnol Oceanogr. Methods 12, 351–362. https://doi.org/10.4319/lom.2014.12.351.
Watanabe, S., Higashitani, N., Tsurushima, N., Tsunogai, S., 1995. Methane in the western North Pacific. J. Oceanogr. 51 (1), 39–60. https://doi.org/10.1007/BF02235935.
Weber, T., Wiseman, N.A., Kock, A., 2019. Global ocean methane emissions dominated by shallow coastal waters. Nat. Commun. 10 (1), 4584. https://doi.org/10.1038/s41467-019-12541-7.
Weller, D.I., Law, C.S., Marriner, A., Nodder, S.D., Chang, F.H., Stephens, J.A., Wilhelm, S.W., Boyd, P.W., Sutton, P.J.H., 2013. Temporal variation of dissolved methane in a subtropical mesoscale eddy during a phytoplankton bloom in the southwest Pacific Ocean. Prog. Oceanogr. 116, 193–206. https://doi.org/10.1016/j.pocean.2013.07.008.
White, M., Mohn, C., 2004. Seamounts: a review of physical processes and their influence on the seamount ecosystem. Oasis Report. http://epic.awi.de/37314/17/OASIS_Oceanography.pdf.
Wiesenburg, D.A., Guinasso, N.L., 1979. Equilibrium solubility of methane, carbon dioxide, and hydrogen in water and sea water. J. Chem. Eng. Data 24 (4), 356–360. https://doi.org/10.1021/je60083a006.
Yang, Z., Qian, Q., Chen, M., Zhang, R., Yang, W., Zheng, M., Qiu, Y., 2020. Enhanced but highly variable bioturbation around seamounts in the northwest Pacific. Deep Sea Res. 156, 103190. https://doi.org/10.1016/j.dsr.2019.103190. Part I.
Ye, W., Zhang, G., Zhu, Z., Huang, D., Han, Y., Wang, L., 2016. Methane distribution and sea-to-air flux in the East China sea during the summer of 2013: impact of hypoxia. Deep-Sea Res. II. 124, 74–83. https://doi.org/10.1016/j.dsr2.2015.01.008.
Ye, W., Wang, X., Zhang, X., Zhang, G., 2020. Methane production in oxic seawater of the western North Pacific and its marginal seas. Limnol. Oceanogr. 65, 2352–2365. https://doi.org/10.1002/lno.11457.
Yoshida, O., Inoue, H.Y., Watanabe, S., Noriki, S., Wakatsuchi, M., 2004. Methane in the western part of the Sea of Okhotsk in 1998–2000. J. Geophys. Res. 109, C09S12. https://doi.org/10.1029/2003JC001910.
You, Y., 2003. The pathway and circulation of North Pacific intermediate water. Geophys. Res. Lett. 30 (24), 2291. https://doi.org/10.1029/2003GL018561.
Zhao, R., Zhao, F., Zheng, S., Li, X., Wang, J., Xu, K., 2022. Bacteria, Protists, and Fungi may hold clues of seamount impact on diversity and connectivity of deep-sea pelagic communities. Front. Microbiol. 13, 773487. https://doi.org/10.3389/fmicb.2022.773487.
Zhao, R., Zhao, F., Feng, L., Fang, J.K.-H., Liu, C., Xu, K., 2023. A deep seamount effect enhanced the vertical connectivity of the planktonic community across 1,000 m above summit. J. Geophys. Res.: Oceans 128 (3), e2022JCO18898. https://doi.org/10.1029/2022JCO18898.